A two-dimensional cochlear fluid model based on conformal mapping

Hannes Lüling[a)]
Computational Neuroscience, Ludwig-Maximilians-Universität München, 82152 Planegg-Martinsried, Germany

Jan-Moritz P. Franosch and J. Leo van Hemmen
Physik Department T35, Technische Universität München, 85747 Garching bei München, Germany

(Received 6 May 2010; revised 28 September 2010; accepted 29 September 2010)

Using conformal mapping, fluid motion inside the cochlear duct is derived from fluid motion in an infinite half plane. The cochlear duct is represented by a two-dimensional half-open box. Motion of the cochlear fluid creates a force acting on the cochlear partition, modeled by damped oscillators. The resulting equation is one-dimensional, more realistic, and can be handled more easily than existing ones derived by the method of images, making it useful for fast computations of physically plausible cochlear responses. Solving the equation of motion numerically, its ability to reproduce the essential features of cochlear partition motion is demonstrated. Because fluid coupling can be changed independently of any other physical parameter in this model, it allows the significance of hydrodynamic coupling of the cochlear partition to itself to be quantitatively studied. For the model parameters chosen, as hydrodynamic coupling is increased, the simple resonant frequency response becomes increasingly asymmetric. The stronger the hydrodynamic coupling is, the slower the velocity of the resulting traveling wave at the low frequency side is. The model's simplicity and straightforward mathematics make it useful for evaluating more complicated models and for education in hydrodynamics and biophysics of hearing.
 [DOI: 10.1121/1.3505108]

PACS number(s): 43.64.Kc, 43.64.Bt [BLM] Pages: 3577–3584

I. INTRODUCTION

Because of its graded stiffness, width, and mass, the cochlear partition, i.e., the basilar membrane together with the organ of Corti, enables its possessor to analyze sound spectra. Besides practical efforts[1,2] to understanding cochlear mechanics, there are several mathematical approaches.[3–11] Not only are the mechanical properties of the cochlear partition the ones that need to be captured but also its intricate interaction with the fluids in which it is immersed. This makes the task a mathematically delicate one.

In order to understand cochlear function as it originates from different parts, it is useful to derive analytic equations for the cochlear partition's motion. Many ways of approximating cochlea mechanics have been discussed so far. Among them are the long-wave approximation[8] and short-wave approximation.[7,9] These theories assume the local wave length of the cochlear partition to be long or short, respectively, as compared to the duct's height. Both assumptions fail either near the resonance region or far away from it.[10] All these approximative theories have been reviewed by Wever[12] and, more recently, by Sieroka who additionally discusses a composition of the long- and short-wave approximation.[10]

Beyond the above approximations there are attempts to solve cochlea partition motion equations in a stricter manner for different dimensions. Grossly unrealistic one-dimensional models can nevertheless give a good prediction of cochlear response,[5] but because of substantial simplifications they prevent studying fluid effects. In order to account for fluid motion more accurately, two-dimensional theories have been put forward, with Siebert's[9] and Allen's[3] leading the way. Deriving integral equations, both enable reducing the problem by one dimension. Both theories' equations are equivalent. Siebert, unlike Allen, has solved it by taking advantage of the short-wave approximation. In an ample review, Lighthill[5] considered Allen's model[3] the best among the two-dimensional ones. Three-dimensional models[13] appear to be analytically unfeasible, as long as dimensionality is not reduced. Much of the three-dimensional work[11,14–18] is enveloped in difficult mathematics that still require simplifying assumptions which deny much of the physiological reality of the cochlea.[19]

In the present paper we present a new two-dimensional cochlear fluid model based on conformal mapping. Although the conformal-mapping method is well-known in fluid dynamics, its application to cochlear modeling is novel. This method is both analytically and numerically simple in comparison to alternative methods, e.g., finite differences and image methods, and does not require approximations that are intrinsic to some methods, e.g., long- and short-wave models. Under the assumptions of an inviscid, irrotational, and incompressible fluid the problem is reduced to solving the Laplace equation for the velocity potential with boundary conditions prescribed by the geometry, as explained in detail in the next paragraph. Applying the technique of conformal mapping simplifies this boundary value problem substantially since it allows for the reduction

[a)]Author to whom correspondence should be addressed. Electronic mail: lueling@bio.lmu.de

of a complicated boundary value problem to an easy one, solely by transforming a known solution through the proper conformal mapping. We then use the velocity potential to determine the force acting on a continuum of damped oscillators representing the cochlear partition. The result is an equation of motion that is exact and entirely analytic within the geometric and hydrodynamic approximations described above. It is solved numerically in order to obtain the time-dependent motion of the cochlear partition, given the acceleration of the stapes. The advantage of an analytically derived equation of motion is that it can be easily modified so that one can investigate the significance of different physical effects on cochlear motion. For instance, the results below confirm that hydrodynamic coupling plays an important role in sharpening the response of the cochlear partition to pure tones. In particular, strengthening hydrodynamic coupling makes the resonant frequency response increasingly asymmetric.

II. THE SIMPLIFIED GEOMETRY

We simplify the difficult three-dimensional problem and assume that the cochlea is an one-sided open two-dimensional box as in Fig. 1. We do so by "unfolding" the cochlea in the following way: First of all, the snail-shaped duct is unrolled so that it becomes straight and has the shape indicated by the dashed lines in Fig. 1. The cochlear partition still divides the duct in the middle such that the two fluid-filled parts are connected by the *helicotrema*. We assume that the exact form of the fluid flow through the helicotrema is negligible so that, in good approximation, we can further unfold the duct along the semi-infinite lines. The result is a rectangular box with one open side representing the round window. The closed side on the opposite end represents the oval window connected to the stapes footplate. The closed side on the left in Fig. 1 is the unfolded bony wall. The closed side on the right consists of twice the cochlear partition. Finally the inward dimension is neglected. As the resulting geometry now represents the cochlea partition *twice*, any motion of the cochlear partition must be symmetric about the point $(H/2, \mathrm{L})$, which is the former apical end of the cochlear partition. Except for one side being open, the resulting model geometry is equivalent to Allen's.[3] One open side approximates the physics of the cochlea better than fully enclosed cavities since the round window is in fact flexible. If it were not, incompressibility would not allow fluid motion at all.

III. THEORY

Elastic coupling between two adjacent parts of the cochlear partition is negligible.[6] Assuming sufficiently small displacements, we can therefore describe the motion of the cochlear partition by a continuum of damped linear oscillators,

$$m(\eta)\frac{\partial^2\gamma}{\partial t^2}(\eta,t)+h(\eta)\frac{\partial\gamma}{\partial t}(\eta,t)+k(\eta)\gamma(\eta,t)=f(\eta,t), \qquad (1)$$

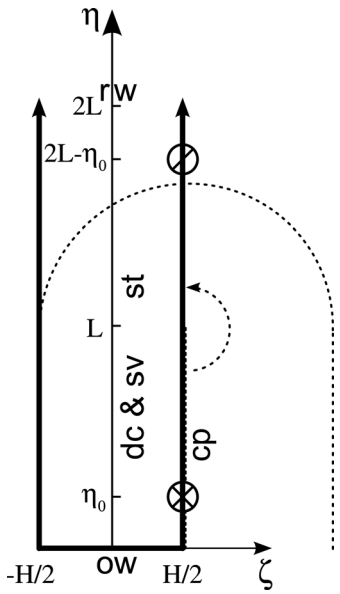

FIG. 1. Cochlear geometry: rw, *round window*; ow, *oval window*; cp, *cochlear partition*; dc and sv, *ductus cochlearis* and *scala vestibuli* unified; st, *scala tympani*. The figure shows an abstract cochlea structure both in its unfolded (solid line) and original (dashed line) shape. For clarity, the length of the cochlea channel L (vertical) is displayed as shorter relative to the height H of the duct (horizontal). The basilar membrane is at position $\zeta = H/2$, the oval window at position $\eta = 0$, the round window at position $\eta = 2L$. The effect of Reissner's membrane (*membrana vestibularis*) is acoustically negligible.[13] We therefore consider the two ducts dc and sv to be identical. We "unfold" the original cochlea structure (dashed lines) along the dashed half-circle shaped arrow so as to get a straight one (solid lines) with effectively open boundary conditions at $\eta = 2L$ instead of the dashed U-turn at originally $\eta = L$. This leads to a double representation of the basilar membrane, namely one from 0 to L and one from L to $2L$. Any motion of the cochlear partition at η_0 (plus in circle) thus coincides with an opposite motion at $2L - \eta_0$ (minus in circle). Motions lead to flux sources and sinks. The round window is represented by an effluent at $2L$.

where $\gamma(\eta, t)$ is the partition's displacement at position η and time t. Mass m, damping h, stiffness k, as well as the external force f are the corresponding quantities per unit of length. Active elements, i.e., the amplification by outer hair cells, are neglected here, albeit they could be introduced for instance as undamping,[20] i.e., as an additional term $-u(\eta)\,\partial\gamma(\eta,\ t)/\partial t$ in Eq. (19). The external force density arises from pressure differences across the cochlear partition and is thus written

$$f(\eta,t)=b\,\Delta p(\eta,t)=b[p(\eta,t)-p(2L-\eta,t)], \qquad (2)$$

where b is the width of the cochlear partition and Δp is the difference between pressure right above and below it. Then, in the unfolded model, $\Delta p(\eta,\ t) = [p(\eta,\ t) - p(2L - \eta,\ t)]$ (see Fig. 1). For simplicity the width and height of the duct are assumed to be constant here. As we will see later, this assumption allows us to create analytic expressions for fluid forces and to better understand the underlying physics without fundamentally changing the cochlea function.

In good approximation, the cochlear fluid is inviscid and incompressible.[13] Accordingly, the Euler equation of fluid motion[21] holds. As fluid motion is approximately irrotational,[13] Bernoulli's equation

$$p = \varrho\left(\frac{\partial\Phi}{\partial t} - \frac{1}{2}\upsilon^2 - V\right) + \text{constant} \tag{3}$$

applies, where υ denotes fluid velocity, p pressure, ϱ fluid density, V the gravity potential, and Φ the velocity potential is determined by

$$\upsilon = -\nabla\Phi. \tag{4}$$

The term υ^2 in Eq. (3) is negligible.[22,23] Taking the divergence on both sides of Eq. (4) and using the incompressibility condition div $\upsilon = 0$ we get the Laplace equation

$$\frac{\partial^2\Phi}{\partial\zeta^2} + \frac{\partial^2\Phi}{\partial\eta^2} = 0. \tag{5}$$

The proper boundary conditions for the box specified in Fig. 1 are given by

$$-\left.\frac{\partial\Phi}{\partial\eta}\right|_{\eta=0} = \upsilon^S, \tag{6a}$$

$$\left.\frac{\partial\Phi}{\partial\zeta}\right|_{\zeta=-H/2} = 0, \tag{6b}$$

$$-\left.\frac{\partial\Phi}{\partial\zeta}\right|_{\zeta=H/2} = \upsilon^C, \tag{6c}$$

where υ^S is the stapes velocity and υ^C the cochlear partition's velocity. Using Bernoulli's equation (3) we rewrite the force density (2) in the form

$$f(\eta,t) = \varrho b\frac{\partial\Delta\Phi}{\partial t}(\eta,t). \tag{7}$$

Since the cochlear partition has zero thickness, the gravity potential V below and above the cochlear partition is identical, therefore $\Delta V = 0$. In our model of the unfolded duct we then have to put

$$\Delta\Phi(\eta,t) = \Phi(\eta,t) - \Phi(2L-\eta,t), \tag{8}$$

as any motion of the cochlear partition at η coincides with an *opposite* motion at $2L-\eta$.

In order to gain an analytic solution of the Laplace equation (5), given the boundary conditions, Eqs. (6a) and (6b), we take advantage of the method of conformal mapping. In the following, we use analytic maps from the complex w-plane where $w = \zeta + i\eta$, into the complex z-plane where $z = x + iy$. Analytic functions are harmonic so that they satisfy the Laplace equation (5), which one can verify with the help of the Cauchy–Riemann equations; cf. Churchill (Ref. 24, Chap. 2) and Titchmarsh (Ref. 25, Secs. 2.13–2.15 and 6.15, Chap. VI). Hence the analytic function

$$u(z) = \phi(z) + i\psi(z), \tag{9}$$

the so-called complex potential, is a solution of the Laplace equation, too. Once we have an analytic function satisfying simple boundary conditions, the theory of conformal mapping allows for transforming the solution to different, and, supposedly, more complicated boundary conditions. Suppose that the conformal function

$$g(w) = x(\zeta,\eta) + iy(\zeta,\eta)$$

maps an arc Γ in the w-plane onto an arc C in the z-plane, then the function

$$U(\zeta,\eta) = u[x(\zeta,\eta), y(\zeta,\eta)]$$

satisfies the corresponding condition along Γ.[24,25]

The conformal map mapping an infinitely long (vertical direction in Fig. 2) box of height H (horizontal direction) in the w-plane, with the side at infinity being open and the opposite side overlapping the real axis (Fig. 1), onto the upper complex half plane is[24]

$$g(w) = H\sin\left(\frac{\pi}{H}w\right). \tag{10}$$

The complex potential of a point source at z_0 with source strength q in an *unbounded* region is

$$\begin{aligned} u(z) &= -\frac{1}{2\pi}q\ln(z-z_0) \\ &= -\frac{1}{2\pi}q[\ln|z-z_0| + i\arg(z-z_0)]. \end{aligned} \tag{11}$$

The complex potential of a distribution of point sources with density $q(z_0)$ along the arc C is therefore

$$u(z) = -\frac{1}{2\pi}\int_C q(z_0)\ln(z-z_0)\,dz_0. \tag{12}$$

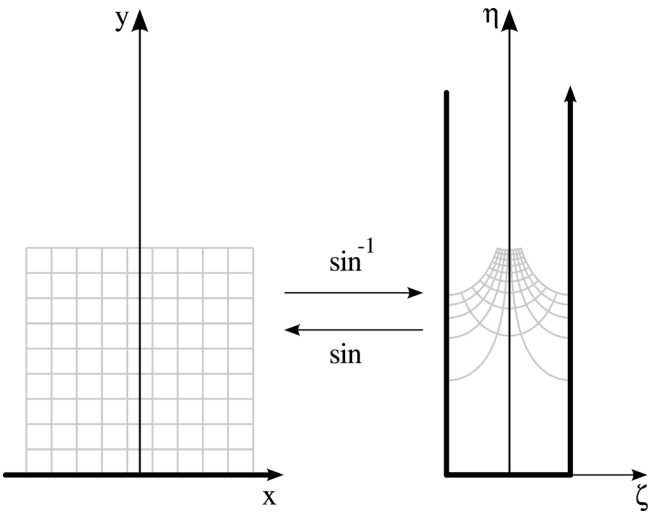

FIG. 2. An illustration of conformal mapping. The sine function maps an infinitely long one-sided open box onto the upper complex half plane.[24] The inverse function maps the upper complex half plane onto the specified box. A globally perpendicular lattice in the upper half of the z-plane (left panel, gray) is thereby mapped onto a new lattice (right panel, gray) within the box in the w-plane, being perpendicular only locally. The x-axis (left panel, thick) is mapped onto the boundary of the specified box (right panel, thick).

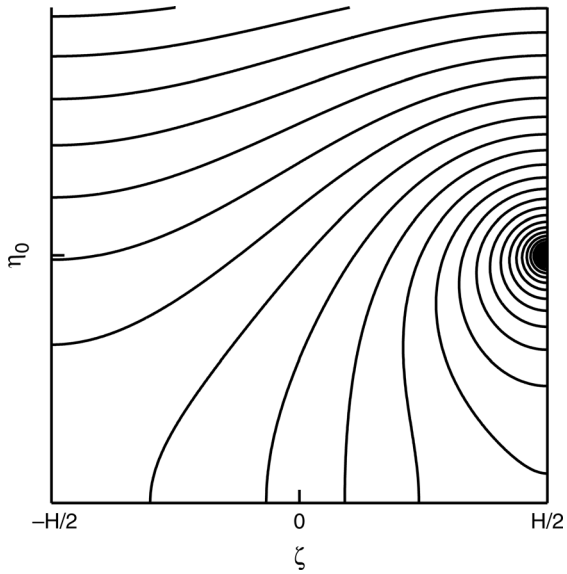

FIG. 3. Iso-potential lines given by $\Phi^C(\zeta, \eta) = \Re[U(w)] = \text{constant}$, generated by a point source at η_0 and a point sink of the same absolute strength at $2L - \eta_0$. Boundary conditions are fulfilled, as every contour hits the box's boundary perpendicularly. We note that the gradient and, hence, the velocity is orthogonal to the contour.

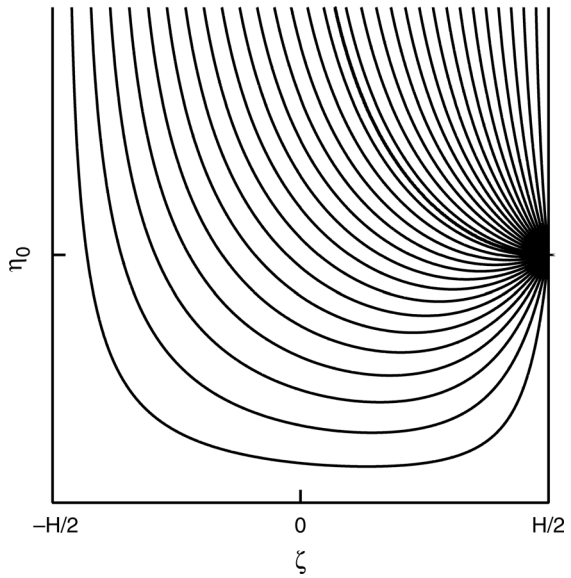

FIG. 4. Stream lines given by $\Psi^C = \Im[U(w)] = \text{constant}$ for different constants, generated by a point source at η_0 and a point sink of the same absolute strength at $2L - \eta_0$. The figure thus describes fluid motion in the cochlea for the case that only one cochlea partition at η_0 moves. The stapes is at position (0,0), the helicotrema at (0,L) far above the visible area.

Thus, according to the theorems above with $z = g(w)$, the complex potential of a distribution of point sources in the one-sided open box is

$$U(w) = -\int_\Gamma Q(w_0) \times \ln\left[\sin\left(\frac{\pi}{H} w\right) - \sin\left(\frac{\pi}{H} w_0\right)\right] \times \cos\left(\frac{\pi}{H} w_0\right) \mathrm{d}w_0, \tag{13}$$

where $Q(w_0)$ is the source distribution along the arc Γ. The factor 1/2 in Eq. (13) has been canceled since only half of a source flows into the box. In Eq. (13) there are sources on the stapes as well as on the cochlear partition. We denote the velocity potentials of the stapes and the cochlear partition by Φ^S and Φ^C, which are the real parts of the corresponding complex potential $U(w)$. Figures 3 and 4 depict contour-plots for point sources. The oval window is part of the real axis and the cochlear partition is represented by the straight line given by $\zeta = H/2$ and $\eta \geq 0$. Using the identities $\sin w = \sin\zeta \cosh\eta + i\cos\zeta \sinh\eta$ and $\cos w = \cos\zeta \cosh\eta - i\sin\zeta \sinh\eta$ we then find

$$\Phi^C(\eta, t) = \int_0^L Q^C(\eta_0, t) K^C(\eta, \eta_0) \sinh\left(\frac{\pi}{H}\eta_0\right) \mathrm{d}\eta_0. \tag{14}$$

The source strength densities $Q^C(\eta_0, t)$ on the cochlear partition result from its motion and thus

$$Q^C(\eta_0, t) = \frac{1}{\pi \sinh\left(\frac{\pi}{H}\eta_0\right)} \frac{\partial\gamma}{\partial t}(\eta_0, t), \tag{15}$$

where the factor $1/\sinh(\pi\eta_0/H)$ undoes the redistribution of the source strength density along the cochlear partition, caused by the transformation $z = g(w)$; cf. Eq. (10). The integration kernel K^C in Eq. (14),

$$K^C(\eta, \eta_0) = -\frac{1}{2\pi}\left[\ln\left|\cosh\left(\frac{\pi}{H}\eta\right) - \cosh\left(\frac{\pi}{H}\eta_0\right)\right| - \ln\left|\cosh\left(\frac{\pi}{H}\eta\right) - \cosh\left(\frac{\pi}{H}(2L - \eta_0)\right)\right|\right], \tag{16}$$

assures that each motion at position η coincides with an opposite one at position $2L - \eta$.

Since a membrane spans the oval window, we may well assume that the stapes, moving with velocity $v^S(t)$, causes a cosine-like source density $v^S(t)\cos(\pi\zeta_0/H)$. In any case a homogeneous flow is present shortly after the basal end. Through an appropriate substitution in Eq. (13) and, again, by considering the nonlinear transformation of sources, we obtain

$$\Phi^S(\eta, t) = -\int_{-H/2}^{H/2} \frac{1}{\pi} v^S(t) \ln\left[\cosh\left(\frac{\pi}{H}\eta\right) - \sin\left(\frac{\pi}{H}\zeta_0\right)\right] \times \cos\left(\frac{\pi}{H}\zeta_0\right) \mathrm{d}\zeta_0. \tag{17}$$

Integrating Eq. (17) we find

$$\Phi^S(\eta, t) = -\frac{H}{\pi} v^S(t)[(\chi + 1)\ln(\chi + 1) - (\chi - 1)\ln(\chi - 1) - 2], \tag{18}$$

where $\chi(\eta) := \cosh(\pi/H\eta)$. For the sake of simplicity we write $\Phi^S(\eta, t) =: Q^S(t)Y^S(\eta)$. As can be seen from Fig. 5, $\Delta Y^S(\eta) := Y^S(\eta) - Y^S(2L - \eta)$ approaches a straight line shortly after the basal end.

Substituting Eqs. (14) and (18) into Eqs. (7) and (1), we obtain an entirely analytic equation of motion for the cochlear partition,

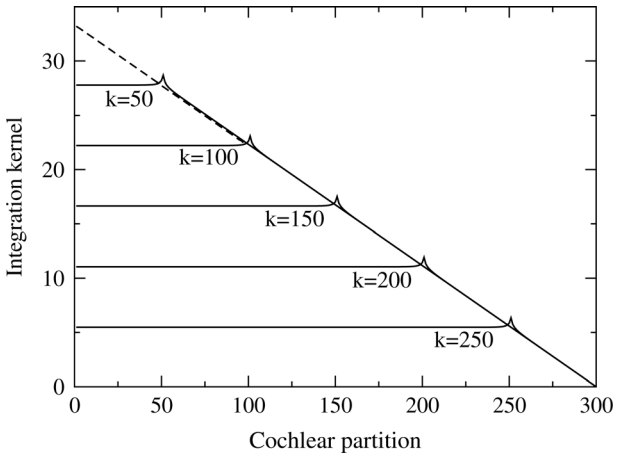

FIG. 5. Each cochlear partition interacts with other cochlear partitions due to hydrodynamic coupling. Strength of hydrodynamic coupling of partition number k acting on partition number j is described by the integration kernel $\Delta\bar{K}^C_{jk}$ in Eq. (22). The solid graphs display $\Delta\bar{K}^C_{jk}$ for different k (50, 100, 150, 200, and 250) depending on the cochlear partition number j, the position. The interaction has a maximum at $j = k$. That is, a cochlear partition interacts maximally with itself, which is physically equivalent to additional mass of the cochlear partition.

$$m(\eta)\frac{\partial^2\gamma}{\partial t^2}(\eta,t)+h(\eta)\frac{\partial\gamma}{\partial t}(\eta,t)+k(\eta)\gamma(\eta,t) = \varrho\, b\,\Delta Y^S(\eta)\frac{\mathrm{d}Q^S}{\mathrm{d}t}(t)+\varrho b\int_0^L\frac{\partial^2\gamma}{\partial t^2}(\eta_0,t)\,\Delta K^C(\eta,\eta_0)\mathrm{d}\eta_0, \tag{19}$$

where $\Delta K^C(\eta,\eta_0) := K^C(\eta,\eta_0) - K^C(2L-\eta,\eta_0)$. Although the original hydrodynamic problem is two-dimensional, we are given a spatially one-dimensional equation of motion and need not solve it for the fluid motion explicitly.

IV. COMPARISON TO THE METHOD OF IMAGES

Allen[3] considered the same geometry used here, except that his boundary conditions do not allow for one of the sides being open, thus neglecting the presence of the round window. Taking advantage of the method of images, he found the Green's function, i.e., the real part of the complex potential generated by the cochlear partition, being given by the infinite sum

$$G^C(x,x_0) = -\frac{(-1)^j}{\pi}\sum_{j=0}^{\infty}\sum_{k=0}^{\infty}\ln[r^+_{j,k}(x,x_0)r^-_{j,k}(x,x_0)] \tag{20}$$

with

$$r^{\pm}_{j,k}(x,x_0) = \sqrt{(x\pm x_0+2jL)^2+(2kH)^2} \tag{21}$$

instead of Eq. (16). The double sum stems from an infinite number of images of point sources and sinks. Since the exact limit of Eq. (20) is unknown, the sum has to be truncated after a few terms. Moreover, when considering stapes motion, the method of images leads to an open duct, which is inconsistent. On the other hand, the method of conformal mapping allows for consistent and physically plausible boundary conditions.

V. NUMERICS

To solve the equation of motion Eq. (19) numerically, the cochlear partition is divided into N equally long elements of length $l = L/N$. The minimal coherence length, i.e., the distance over which a transversal section of the membrane will appear to move as a single structure, is about 120 μm.[26] Finer discretization would make the model less realistic. As others[27] have, we therefore chose a total of $N = 300$ elements.

Each of those elements is indicated by j or k, such that $\eta = jl$ and $\eta_0 = kl$.

With η approaching η_0, $\Delta K^C(\eta,\eta_0)$ diverges. Thus one has to average the kernel by numerical integration in the neighborhood of these singular points,

$$\Delta\bar{K}^C_{jk} := \frac{1}{l}\int_{(k-1/2)\,l}^{(k+1/2)\,l}\Delta K^C(jl,\eta_0)\,\mathrm{d}\eta_0. \tag{22}$$

Correspondingly the averaged stapes-cochlear interaction is defined by

$$\Delta\bar{Y}^S_j := \frac{1}{l}\int_{(j-1/2)\,l}^{(j+1/2)\,l}\Delta Y^S(\eta_0)\,\mathrm{d}\eta_0. \tag{23}$$

To compute $\Delta\bar{Y}^S_j$ numerically using Eq. (18), which contains the term $\chi[\ln(\chi+1)-\ln(\chi-1)]$, we have replaced this term by its limit 2 for $\chi > 10^6$ to avoid numerical instability. Upon introducing a mass matrix $\boldsymbol{M}$ with components

$$M_{jk} := \delta_{jk}m_k + \varrho\, l\, b\,\Delta\bar{K}^C_{jk} \tag{24}$$

and a vector $\boldsymbol{q}$ with components

$$q_j\left(\frac{\mathrm{d}\gamma_j}{\mathrm{d}t}(t),\gamma_j(t),t\right) := \varrho\, b\,\Delta\bar{Y}^S_j\frac{\mathrm{d}v^S}{\mathrm{d}t}(t) - h\frac{\mathrm{d}\gamma_j}{\mathrm{d}t}(t) - k_j\gamma_j(t), \tag{25}$$

we can reduce the discretized counterpart of Eq. (19)

$$\frac{\mathrm{d}^2\gamma}{\mathrm{d}t^2}(t) = \mathbf{M}^{-1}\,\boldsymbol{q}\left(\frac{\mathrm{d}\gamma}{\mathrm{d}t}(t),\gamma(t),t\right). \tag{26}$$

Together with the initial values

$$\frac{\mathrm{d}^2\gamma}{\mathrm{d}t^2}(t_0) = \mathbf{M}^{-1}\,\boldsymbol{q}\left(\frac{\mathrm{d}\gamma}{\mathrm{d}t}(t_0),\gamma(t_0),t_0\right), \tag{27a}$$

$$\frac{\mathrm{d}\gamma}{\mathrm{d}t}(t_0) = 0, \tag{27b}$$

$$\gamma(t_0) = 0, \tag{27c}$$

this results in an initial value problem that we have solved by a second order Runge–Kutta method.[28]

Each time step requires a multiplication of a vector of length N by the symmetric $N \times N$ matrix $\boldsymbol{M}^{-1}$ and therefore has the same computational complexity as all models that

TABLE I. The parameters used in the simulations were taken from Mammano and Nobili,[6] except for the width of the cochlear partition, which was taken to be constant, and the stiffness k, which was adapted to the frequency range of human hearing. We approximated the viscosity h by a linear function. The values could likewise be replaced by those of other species.

Quantity	Value	Quantity
N	300	Number of elements of the cochlear partition
L	33.5×10^{-3} m	Length of the cochlear partition
ϱ	10^{-3} kg/m^3	Density of the cochlear fluid
H	10^{-3} m	Height of the duct
b	0.2×10^{-3} m	Width of the elements
m_k	$1.7 \times 10^{-4}\, e^{85\mathrm{kL/N}}$ kg/m	Mass per length of the kth strip
h_k	$0165 - 0.1k$/N kg/(ms)	Damping per length of the cochlear fluid
k_k	$2.8 \times 10^{6}\, e^{-10.13\ \mathrm{k/N}}$ kg/(ms^2)	Stiffness per length of the kth strip
a	10^{-9} m	Stapes amplitude
v^S	$a\omega \cos(\omega t)$	Stapes velocity

integrate Eq. (26). The condition number of $\boldsymbol{M}$ is approximately 498 and remains about the same even for larger N (525 for $N = 1000$, 534 for $N = 3000$, 537 for $N = 10\,000$, and 538 for $N = 30\,000$).

The simulation code in C++ is available on request to the authors. The parameters used for all graphs are listed in Table I. Figure 5 shows $\Delta\bar{K}^C_{jk}$. The cochlea maps different frequencies to different positions along the basilar membrane as in the simulations shown in Fig. 6.

The phases are mostly monotone functions of the cochlear position, as shown by Fig. 7, evoking the illusion of a wave traveling from stapes to helicotrema. Figure 7 also depicts the frequency dependence of the phase difference. The higher the frequency of the stimulus tone, the higher the maximum phase difference of resonating elements of the cochlear partition.

The presented model reproduces essential cochlear features, viz., frequency selectivity, asymmetry of the envelope

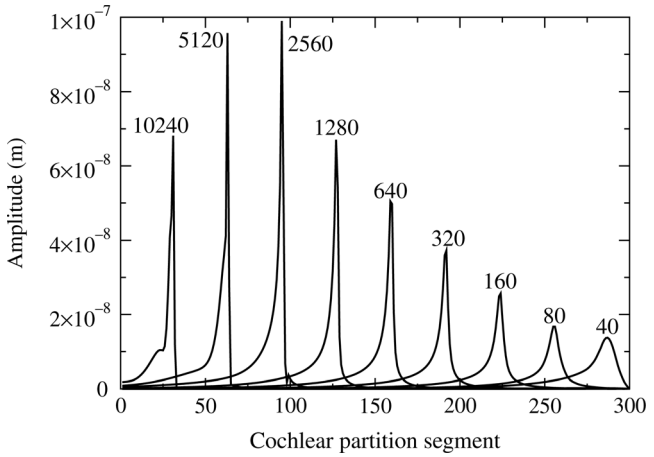

FIG. 6. Amplitude of cochlear partition displacements in dependence upon the position of the cochlear partition (element numbers 1–300) corresponding to the given frequencies (Hz) indicated at the maxima. The cochlea was excited by pure tones, starting with 20 Hz and doubling up to 10 240 Hz which shows the approximately logarithmic dependence of maximal amplitude upon the distance from the helicotrema at partition number 300.

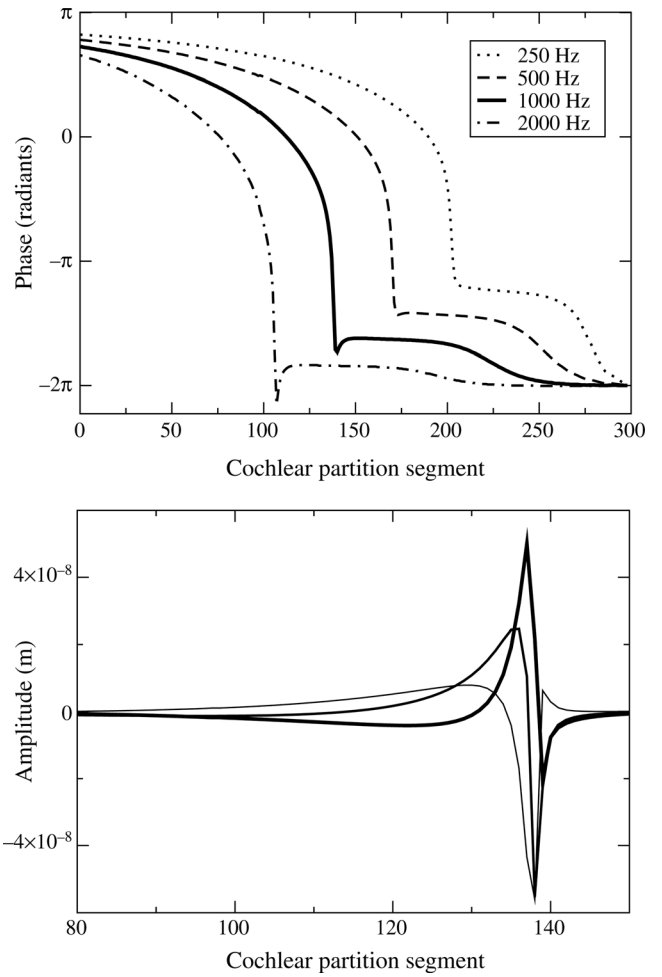

FIG. 7. Upper panel: Phase of cochlear partition displacements in dependence upon the element number of the cochlear partition (1–300) for pure tone stimulations of 250, 500, 1000, and 2000 Hz. The mostly monotonically decreasing phases produce partition displacements such that waves seem to travel from base to apex. Lower panel: Displacement of cochlear partitions in dependence upon the element number of the cochlear partition (1–300) for pure tone stimulation with 1000 Hz for three successive moments of time (thin line, middle line, and thick line) with a time interval of 0.2 ms. For the observer, a wave seems to travel in the direction from stapes (left) to helicotrema (right).

and a mostly monotonic phase. Deviations from previous results, i.e., places of resonance or phase differences of the traveling wave (two cycles[6] for 3.2 kHz input frequency, three cycles[3] for 1 kHz), are possibly due to the choice of functions of mass, damping, and stiffness, which vary among species anyway, even between individuals. For a review of specific phase differences, see Ref. 29. Moreover, different boundary conditions, particularly modeling of the round window as an open end of the duct, may also account for deviating results and need to be studied more accurately in the future.

VI. VARYING HYDRODYNAMIC COUPLING

Besides obvious reasons like shock absorbance and ion supply to hair cells, the cochlear fluid is supposed to improve frequency selectivity. By simple alteration of Eq. (24), we are able to quantitatively study the role of the cochlear fluid in regard to frequency selectivity. Thus, in order to understand the effect of coupling of the cochlea partition to itself

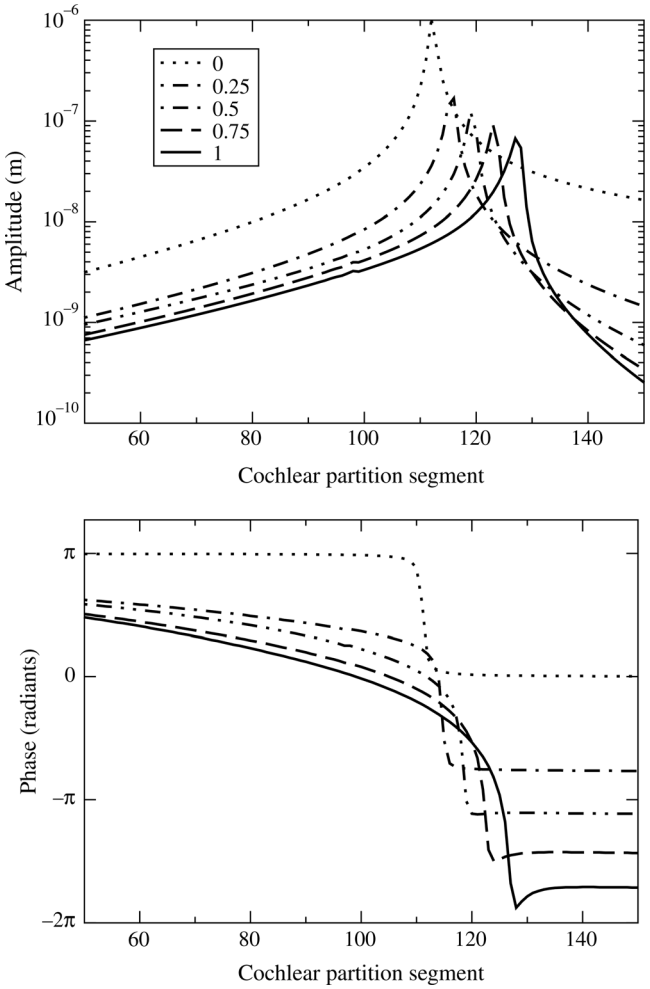

FIG. 8. Upper part: Envelopes of cochlear partition amplitudes for pure tone stimulation with 1280 Hz for different values of hydrodynamic coupling c on a logarithmic scale. The absolute values of the slopes clearly increase with stepwise increasing coupling via the fluid. The sharpening takes place mostly at low frequencies (here the right-hand side). Amplification thereby decreases. Lower part: The corresponding phases show that in case of no hydrodynamic coupling ($c = 0$) there is no traveling wave as the phase is constant except for a small range near the resonance frequency. The stronger hydrodynamic coupling, the lower the velocity of the resulting traveling wave at the low frequency side as the slope of the phase becomes steeper.

through the cochlear fluid, we replace $\bar{K}^C_{jk}$ for $j \neq k$ by $c \cdot \bar{K}^C_{jk}$ in Eq. (24), retaining the diagonal elements and reducing the influence of hydrodynamic coupling by off-diagonal elements for a coupling parameter $0 \leq c < 1$. Figure 8 shows the effect of hydrodynamic coupling of different cochlear partition segments by gradually reducing the coupling parameter c. Hydrodynamic coupling sharpens the frequency response, especially at the low frequency side. It also shifts the position of maximal displacement to the low frequency side. The peak of the dotted graph in Fig. 8 is almost symmetric as it is just the response of harmonic oscillators with varying resonance frequencies arranged along the cochlea.

VII. DISCUSSION

The main purpose of this article is to introduce a new base model of the cochlea, and accordingly some advantages and disadvantages are now pointed out.

Although a two-dimensional cochlear fluid is presumed, the equation of motion is one-dimensional. That is due to the proper positioning of the two arcs representing the oval window and the cochlear partition in the complex plane. Numerics can thus be implemented in a very straightforward way. In a comparative essay, Egbert de Boer (Ref. 30, Chap. 5) found numerical accuracy of the solution difficult to predict or to control for the three-dimensional case.

The cost of computation has decreased drastically in the years since the advent of two-dimensional cochlear models. Nevertheless, efficient computability is still important. Computing the cochlear response in real time, potentially with limited available computing power, and studying parameter dependency requires fast and simple models. Designing hardware implementations[2] requires fast estimates of implications of parameter modifications. In particular, it is not only single parameters that often have to be matched but also parameter functions, which makes the problem variational and computationally costly. In this way the present model can turn out to be a useful tool supplementing existing one-dimensional models.[3,6,26] As it solves a simplified geometry exactly, it may also be used to evaluate finite element models. It can also serve as an initial point for further research as it is easy to implement and to compute.

The model's simplicity also makes it useful as an example in lectures on hydrodynamics. Students may well benefit from this straightforward application of mathematics to biology.

In the present model the helicotrema is not neglected as for example in the models of Steele and Taber[11] or Lesser and Berkeley,[4] since unfolding the cochlea makes the helicotrema part of the straight duct. The round window is consistently modeled as an open end, which is more realistic than a closed box.[3]

But the present technique also has its shortcomings. Conformal mapping restricts all problems to two dimensions. Finding conformal mappings analytically for more realistic cochlea geometries leads to integrals that cannot by solved analytically anymore. The variation of the cochlea scalae, however, is of negligible importance as compared to those the cochlear partition.[13] It also seems unfeasible to include elastic properties of the round window. Yet, the displacement of the round window may well be small enough to neglect its elastic effect.

All in all, we have an analytical derivation of a cochlear equation of motion that opens up a gateway to efficiently handling a multitude of fascinating intrinsic dynamical patterns such as what role hydrodynamic coupling effectively plays and how it can be treated analytically.

ACKNOWLEDGMENTS

The authors like to thank Michael Brunnhuber, Andreas Vollmayr, and Paul Friedel for the scientific discussions and Colin Stoneking for his support concerning language. The work was in part supported by the Bernstein Center for Computational Neuroscience (BCCN) Munich as well as the European Commission, Future and Emerging Technologies (CILIA).

[1]G. Bekesy, "Experiments in hearing," J. Acoust. Soc. Am. **88**, 2905 (1990).
[2]W. Hemmert, U. Düring, M. Despont, U. Drechsler, G. Genolet, P. Vettinger, and D. M. Freeman, "A life-sized, hydrodynamical, micromechanical inner ear," in *The Biophysics of the Cochlea* (World Scientific, Singapore, 2003).
[3]J. B. Allen, "Two-dimensional cochlear fluid model: New results," J. Acoust. Soc. Am. **61**, 110–119 (1976).
[4]M. B. Lesser and D. A. Berkley, "Fluid mechanics of the cochlea. Part 1," J. Fluid Mech. **51**, 497–512 (1972).
[5]J. Lighthill, "Energy flow in the cochlea," J. Fluid Mech. **106**, 149–213 (1981).
[6]F. Mammano and R. Nobili, "Biophysics of the cochlea: Linear approximation," J. Acoust. Soc. Am. **93**, 3320–3332 (1993).
[7]O. F. Ranke, "Theory of operation of the cochlea: A contribution to the hydrodynamics of the cochlea," J. Acoust. Soc. Am. **22**, 772–777 (1950).
[8]M. R. Schroeder, "An integrable model for the basilar membrane," J. Acoust. Soc. Am. **53**, 429–434 (1973).
[9]W. M. Siebert, "Ranke revisited—A simple short-wave cochlear model," J. Acoust. Soc. Am. **56**, 594–600 (1974).
[10]N. Sieroka, H. G. Dosch, and A. Rupp, "Semirealistic models of the cochlea," J. Acoust. Soc. Am. **120**, 297–304 (2006).
[11]C. R. Steele and L. A. Taber, "Comparison of WKB and finite difference calculations for a two-dimensional cochlear model," J. Acoust. Soc. Am. **65**, 1001–1006 (1979).
[12]E. G. Wever, "Development of traveling-wave theories," J. Acoust. Soc. Am. **9B**, 1319–1324 (1962).
[13]M. A. Viergever, *Mechanics of the Inner Ear* (Delft University Press Delft, The Netherlands, 1980), Chaps. 2 and 3.
[14]C. R. Steele, "Behavior of the basilar membrane with pure-tone excitation," J. Acoust. Soc. Am. **55**, 148–162 (1974).
[15]C. R. Steele and L. A. Taber, "Three-dimensional model calculations for guinea pig cochlea," J. Acoust. Soc. Am. **69**, 1107–1111 (1981).
[16]M. H. Holmes, "An analysis of a low-frequency model of the cochlea," J. Acoust. Soc. Am. **68**, 482–488 (1980).
[17]E. de Boer, "The 'inverse problem' solved for a three-dimensional model of the cochlea. I. Analysis," J. Acoust. Soc. Am. **98**, 896–903 (1995).
[18]E. de Boer, A. L. Nuttall, and C. A. Shera, "Wave propagation patterns in a 'classical' three-dimensional model of the cochlea," J. Acoust. Soc. Am. **121**, 352–362 (2007).
[19]H. L. Hawkins, T. A. McMullen, A. N. Popper, and R. R. Fay, editors, *Auditory Computation* (Springer, New York, 1996), Chap. 3.
[20]R. Nobili and F. Mammano, "Biophysics of the cochlea II: Stationary nonlinear phenomenology," J. Acoust. Soc. Am. **99**, 2245–2255 (1996).
[21]H. Lamb, *Hydrodynamics*, 6th ed. (Cambridge University Press, Cambridge, 1932), Chap. 1.
[22]M. A. Viergever and J. J. Kalker, "On the adequacy of the Peterson-Bogert model and on the effects of viscosity in cochlear dynamics," J. Eng. Math. **8**, 149–156 (1974).
[23]M. A. Viergever and J. J. Kalker, "Localization of non-linearities in the cochlea," J. Eng. Math. **9**, 11–20 (1975).
[24]R. V. Churchill, J. W. Brown, and R. F. Verhey, *Complex Variables and Applications*, 3rd ed. (McGraw-Hill, New York, 1974), Chaps. 2 and 8.
[25]E. C. Titchmarsh, *The Theory of Functions*, 2nd ed. (Oxford University Press, Oxford, 1939), Chap. VI, Secs. 2.13–2.15 and 6.15.
[26]R. Nobili, F. Mammano, and J. Ashmore, "How well do we understand the cochlea?," Trends Neurosci. **21**, 159–167 (1998).
[27]P. Mistrik, C. Mullaley, F. Mammano, and J. Ashmore, "Three-dimensional current flow in a large-scale model of the cochlea and the mechanism of amplification of sound," J. R. Soc., Interface **6**, 279–291 (2009).
[28]W. H. Press, S. A. Teukolsky, W. T. Vetterling, and B. P. Flannery, *Numerical Recipes in C* (Cambridge University Press, Cambridge, UK, 1995), Chap. 16.1.
[29]L. Robles and M. A. Ruggero, "Mechanics of the mammalian cochlea," Physiol. Rev. **81**, 1305–1352 (2001).
[30]*The Cochlea, Volume 8 of Springer Handbook of Auditory Research*, edited by P. Dallos, A. N. Popper, and R. R. Fay (Springer, New York, 1996), Chap. 5.